THE FLUX AND THE COMPOSITION OF ULTRA HIGH ENERGY COSMIC RAYS MEASURED BY THE PIERRE AUGER OBSERVATORY

I. C. MARIŞ for the Pierre Auger Collaboration
Institut für Experimentelle Kernphysik, Universität Karlsruhe (TH), Postfach 6980, 76128 Karlsruhe

The cosmic ray flux above 10^{18} eV has been measured with high statistics by the Pierre Auger Observatory. At high energies the flux is suppressed and the hypothesis of a single power-law behavior as obtained in the lower energy range is rejected with a significance of more than 6 sigma. The measurement of the shape of the energy spectrum of ultra high energy cosmic rays can constrain acceleration models only when combined with a composition determination. The fluorescence detector measurement of the longitudinal development of air showers is used to determine the cosmic ray composition and the surface detector data are used to derive upper limits on the flux of photons and tau neutrinos.

Introduction

In the near future the wealth of data recorded by the Pierre Auger Observatory will help to answer some of the main questions in ultra high energy cosmic ray (UHECR) physics, such as their origin and composition. Due to the Greisen-Zatsepin-Kuzmin effect (GZK) [1,2] a flux suppression is expected in the highest energy range, mainly caused by the energy loss of cosmic rays interacting with the microwave background radiation. This has been seen both by the Pierre Auger Observatory [3] and by the HiRes collaboration [4]. Through the hybrid technique of observing the same air showers with two different detectors, the nearly calorimetric estimation of the energy of the primary particle as obtained from the fluorescence technique is transfered to the large number of events recorded by the surface detector. This method is described below in section 1 and the resulting energy spectrum in section 2.

The excess of cosmic rays above the energy threshold given by the GZK effect, as reported by the AGASA experiment [5] might be explained in the so-called *top down* models. In some of these scenarios the origin of cosmic rays is at relatively close distances to the Earth and therefore

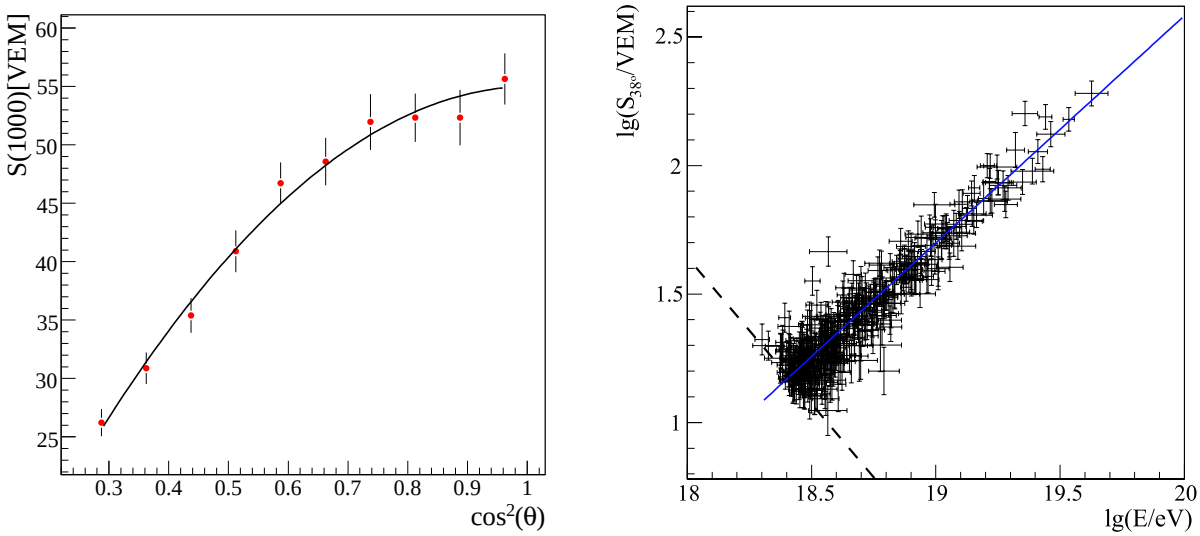

Figure 1: (left hand side) S(1000) attenuation in the atmosphere. The line represents an empirical fit that is used for the conversion to S_{38}. (right hand side) Energy calibration. The events at low energies (below the dashed line) have been rejected to avoid threshold effects. The relation between S_{38} and energy is almost linear and is shown with the continuous line [3].

a large photon content in the cosmic ray flux is predicted at the highest energies. Limits on photon content are presented in section 3 below.

1 Energy calibration

The Pierre Auger Observatory, located in the province of Mendoza (Argentina), is used to measure the properties of extensive air showers by observing their longitudinal development in the atmosphere as well as their lateral spread at ground level. The Observatory consists of 1600 water-Cherenkov detectors(SD), filled with 12 tonnes of water each and equipped with three photomultipliers to detect secondary photons and charged particles. The tanks are spread over 3000 km^2 on a triangular grid of 1.5 km spacing. The atmosphere above the array is viewed by 4 fluorescence detectors (FD), each housing 6 telescopes, located on the border of the area. The field of view of each telescope is 30° in azimuth, and $1.5-30°$ in elevation. Light is focused with a spherical mirror of 11 m^2 effective area on a camera of 440 hexagonal pixels. Each pixel is a photomultiplier tube with 18 cm^2 detection area. More details on detector setup and calibration can be found in [6,7].

After entering the atmosphere, cosmic rays interact with nuclei in the air and start creating extensive air showers. The muons, electrons and photons that reach the ground are detected with the SD, their lateral spread from the air shower axis at primary energies above 10^{18} eV being in the order of a few kilometers. On the way through the atmosphere charged particles excite nitrogen molecules, which afterwards emit fluorescence light in the ultra-violet band. The amount of light is proportional to the energy deposited by the air shower in the atmosphere and is detected with the FD.

The SD has a high duty cycle of almost 100 %, but the energy calibration can be inferred in a model-independent way only from the FD energy assignment [8]. The detected signal at 1000 m from the shower axis on the ground level, S(1000), is a good estimator for the energy of the cosmic ray. Due to the attenuation in the atmosphere, S(1000) depends on the zenith angle: an air shower developing vertically produces a smaller signal than an inclined shower produced by

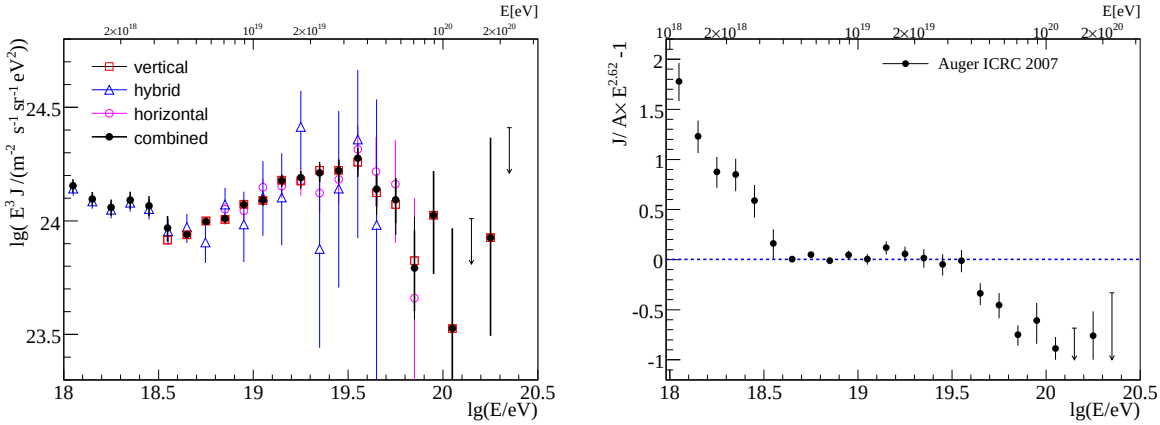

Figure 2: (left hand side) Flux multiplied by E^3 derived from hybrid data set (opened triangles) together with the spectra obtained from the SD using showers with zenith angles of less than 60° (opened squares) and more than 60° (opened circles). The Auger combined energy spectrum is denoted by filled circles. Only statistical uncertainties are shown. Arrows indicate 84% CL upper-limits. (right hand side) Fractional difference between the Auger spectrum and an assumed flux $\propto E^{-2.6}$ as a function of energy.

a cosmic ray with the same energy. The constant intensity method [3] is applied to obtain the zenith angle correction : it assumes that the cosmic ray flux is isotropic in local coordinates, i.e. the number of events above a certain threshold energy is constant as a function of $\cos^2\theta$. This hypothesis leads to the correction function for S(1000) shown in Fig. 1(left). A new variable obtained by using the empirical fit shown in the same figure, S_{38}, represents the signal at 1000 m the very same shower would have produced if it had arrived from a zenith angle of 38°. This angle corresponds to the median of the zenith angle distribution of the SD data. The number of events above a certain S_{38} is zenith angle independent. In principle the attenuation might be energy dependent, because showers with higher energies develop deeper in the atmosphere and can be observed before their maximum development. This effect was found to be negligible.

The transformation from S_{38} to energy is obtained from high quality hybrid events. These are air showers that triggered both SD and FD, so S(1000) and FD energy have been reconstructed with good accuracy. The relation between the two variables, shown in Fig. 1 (right), exhibits a power law correlation with a relative dispersion of $19 \pm 1\%$. The uncertainties in the determination of both FD energy and SD signal are assigned on event by event basis.

2 Ultra high energy cosmic ray flux

The data collected at the Pierre Auger are divided in three sets. The first set consists of air showers with zenith angle of less than 60° detected by SD. The energy calibration described above is applied in this case. The integrated exposure reported here is 5165 km^2 sr yr after some quality cuts (through February 2007), more than a factor of three larger than the exposure obtained by the largest forerunner experiment AGASA [5]. (Elsewhere in these Proceedings, Bonino reports other Auger results using an exposure through August 2007 of 9000 km^2 sr yr). The acceptance is computed by simple geometrical considerations and from the continuous monitoring of the configuration of the array [9]. The data set used for obtaining the energy spectrum contains only events with energies greater than $3 \cdot 10^{18}$ eV; above this energy the array is fully efficient.

The second set contains air showers measured by the SD with a zenith angle between 60° and 80°. The procedure to derive the energy is equivalent to the vertical events, but instead of using S_{38} the shower size is determined from the relative distributions of the two-dimensional muon number densities at ground level. The normalization factor of the muon map, N_{19}, is the estimator to be related to the hybrid energy. It gives the total number of muons relative

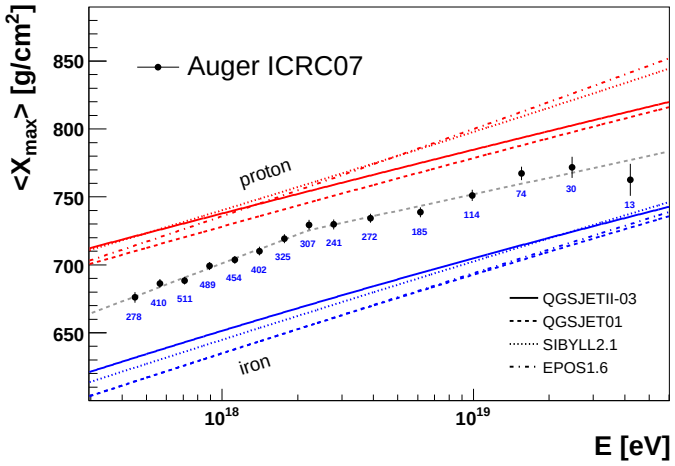

Figure 3: The mean of $X_{\max}$ distribution as a function of energy [13] together with predictions from Monte Carlo simulations. Event numbers are indicated below each data point.

to a shower initiated by a proton with an energy of 10^{19} eV. The acceptance calculation is purely geometrical and the threshold energy above which the trigger efficiency is more than 98% is $6.3 \cdot 10^{18}$ eV. Above this energy the integrated exposure until the end of February 2007 is 1510 km^2 sr yr; 29% of the equivalent acceptance for vertical events [11].

The remaining set comprises of showers detected by the fluorescence detector and at least one SD unit. The hybrid exposure calculation relies on the simulation of the FD and SD response and it is energy dependent. A large sample of Monte Carlo simulations are performed to reproduce the exact conditions of the experiment and the entire sequence of given configurations, for example the rapidly growing array, as well as the seasonal and instrumental effects. The advantage of the hybrid measurement of the energy spectrum [12] is the coverage of the energy range between 10^{18} eV and $3 \cdot 10^{18}$ eV.

The energy spectra obtained with the three methods are illustrated in Fig. 2 (left). The agreement is well within the independent systematic uncertainties, the difference between the overall normalizations is at a level of less than 4%. All spectra are affected by the 22% uncertainty in the FD energy scale, the main contributions coming from the determination of the fluorescence yield (14%), from the energy reconstruction itself (10%) and from the absolute calibration of the detector (9.5%). This systematic uncertainty does not affect the relative comparison of the three spectra. In order to obtain the Auger energy spectrum extending over the widest energy range possible, a maximum likelihood method is applied taking into account the independent uncertainties of each measurement [10]. The systematic uncertainty in the hybrid spectrum is dominated by the calculation of the exposure and reaches 20% in the low energy range. The systematic uncertainties of the SD spectra have contributions from the acceptance determination (3%) and from the conversion of S(1000) and N_{19} to energy ($< 10\%$).

In Fig. 2 (right) is illustrated the fractional difference between the Auger spectrum and a power-law $\propto E^{-2.6}$ which corresponds to the behavior of the energy spectrum between 18.6 and 19.6 in log(E/eV). Two spectral features are clearly visible: the so-called *ankle* at energies of $\approx 10^{18.5}$ eV and a flux suppression at energies above $\approx 10^{19.6}$ eV. The spectral index changes from $\gamma_1 = -3.30 \pm 0.06$ to $\gamma_2 = -2.62 \pm 0.03(\text{stat}) \pm 0.02(\text{sys})$ at $\log(E_{\text{ankle}}/\text{eV}) = 18.65 \pm 0.04$, and above $10^{19.6}$ eV to $\gamma_3 = -4.14 \pm 0.42(\text{stat})$. A continuation of the energy spectrum as a power law with index γ_2 predicts 132 ± 9 events above $10^{19.6}$ eV and 30 ± 2.5 above 10^{20} eV, whereas we observe only 51 events and 2 events. The hypothesis of a pure power-law can be rejected with a significance of 6σ.

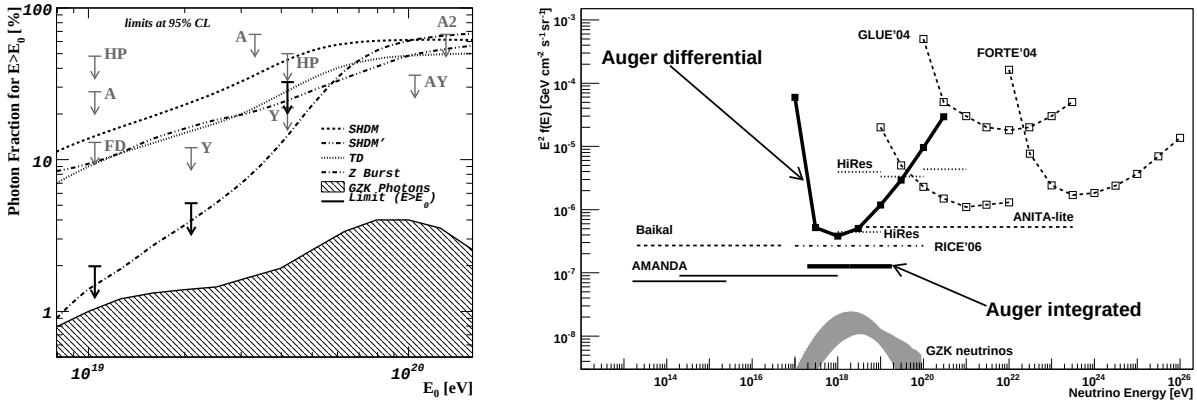

Figure 4: (left hand side) The upper limits on the fraction of photons in the integral cosmic ray flux (black arrows) along with the previous experimental limits. Also shown are the predictions from top-down models (SHDM, TD and ZB, SHDM) and with predictions of the GZK photon fraction (see [14] and ref. therein). (right hand side) Limits at 90% C.L. for a diffuse flux of ν_τ (see [15] and ref. therein).

3 Mass composition

Spectral features alone cannot constrain acceleration models. Additionally the mass of the arriving particles has to be determined. Observables related to the shower development are used to identify the nature of the primary particles. At a given energy showers from a heavier nuclei develop earlier in the atmosphere, leading to different footprints in the array or the camera.

One variable sensitive to the composition of the cosmic rays is the slant depth position $X_{\max}$ at which the maximum of the longitudinal profile occurs. Its average value is related linearly to the mean logarithmic mass, $\langle \ln A \rangle$, at a certain energy E: $\langle X_{\max} \rangle = D_p[\ln(E/E_0) - \langle \ln A \rangle] + c_p$. D_p is referred to as *elongation rate* and c_p is the average depth of a proton with energy E_0. Showers observed by at least one fluorescence detector and with at least one triggered tank were used to derive the mass composition of the cosmic rays [13]. The mean $X_{\max}$ as a function of energy together with predictions from air shower simulations is shown in Fig. 3 (left). The $X_{\max}$ uncertainty is less than $20\,\mathrm{g/cm^2}$. A moderate lightening of the primary composition is observed up to $\approx 2.5 \cdot 10^{18}\,\mathrm{eV}$, indicated by a slope larger than that of either pure proton or pure iron, whereas a constant mixed composition is present at high energies. The highest energy cosmic rays seem to develop higher in the atmosphere, indicating a heavy composition, or at least not a pure proton one. Larger statistics or independent analysis of the fluctuations of $X_{\max}$ and SD mass composition estimators are needed to strengthen these results.

Photon induced showers have a strong individuality compared to the showers induced by nuclei. They develop slower in the atmosphere having a larger $X_{\max}$. The main reason is the smaller multiplicity in the electromagnetic interactions compared to the hadronic ones combined with the LPM effect. Photon showers also contain fewer secondary muons, which combined with the deep penetration in the atmosphere leads to large rise times of the signal in the SD tanks and to a shower front with a larger curvature than hadronic showers. These two parameters are combined into a single SD observable through the principal component analysis to maximize the discrimination power [14]. The Pierre Auger collaboration has derived a direct limit on the flux of photons for the first time by searching for photon candidates and relating their number to the exposure of the surface array. No photons have been found in the Auger data and therefore only limits on the photon fraction are shown in Fig. 4 (left). These limits improve significantly upon bounds from previous experiments, excluding some top down models as the super-heavy dark matter scenario. The flux expected for GZK photons will be reached with data accumulating

over the next years.

In the case of the topological defects models, the UHECRs sources are distributed all over the universe and most of the high energy photons interact with the cosmic microwave background. The photon flux at Earth would be low in this scenario while the neutrino flux is not attenuated. The upper limit on the diffuse flux of ultra high energy tau neutrinos, presented in Fig. 4 (right), was built based on the search for neutrinos with the characteristics of extremely inclined, deeply penetrating events with a large electromagnetic component [15]. The Pierre Auger Observatory is most sensitive to Earth-skimming ν_τ in the energy range where the GZK neutrinos are expected. The derived limit in the energy range $2 \cdot 10^{17}$- $2 \cdot 10^{19}$ eV is at present the most sensitive bound.

4 Conclusions

The southern Pierre Auger Observatory will be completed at the end of 2008. Already with a data set that is comparable to the statistics of one year fully operational array, the hypothesis of a continuation of the energy spectrum in the form of a power law above an energy of $10^{19.6}$ eV is rejected with 6 sigma significance. This result is independent of the energy scale uncertainties. Combined with the directional correlation of the highest energetic cosmic rays with nearby active galactic nuclei [16] the observed flux suppression suggests the existence of a GZK-effect. A mixed composition of the cosmic rays is present over the whole energy range and upper limits on photon and neutrino fluxes are given. The nature of the highest energies will be determined more precisely within the following year with increased statistics and different observables.

References

1. K. Greisen, *Phys. Rev. Lett.* **16**, 748 (1966).
2. G.T. Zatsepin and V.A. Kuz'min, *JETP Lett.* **4**, 78 (1966).
3. M. Roth [Pierre Auger Collaboration], *Proc. 30th ICRC, Mérida* (2007), arXiv:0706.2096v1 [astro-ph].
4. R.U. Abbasi *et al.*, *Phys. Rev. Lett.* **100**, 101101 (2008).
5. M. Takeda *et al.*, *Astropart. Phys.* **19**, 447 (2003).
6. J. Abraham *et al.* [Pierre Auger Collaboration], *Nucl. Instrum. Methods* A **523**, 50 (2004).
7. X. Bertou *et al.* [Pierre Auger Collaboration], *Nucl. Instrum. Methods* A **568**, 839 (2006).
8. M. Unger *et al.*, *Nucl. Instrum. Methods* A **588**, 433 (2008).
9. D. Allard [Pierre Auger Collaboration], *Proc. 29th ICRC, Pune* **7**, 287 (2005).
10. T. Yamamoto [Pierre Auger Collaboration], *Proc. 30th ICRC, Mérida* (2007), arXiv:0707.2638 [astro-ph].
11. P. Facal San Luis [Pierre Auger Collaboration], *Proc. 30th ICRC, Mérida* (2007), arXiv:0706.4322 [astro-ph].
12. L. Perrone [Pierre Auger Collaboration], *Proc. 30th ICRC, Mérida* (2007), arXiv:0706.2643 [astro-ph].
13. M. Unger [Pierre Auger Collaboration], *Proc. 30th ICRC, Mérida* (2007), arXiv:0706.1495v1 [astro-ph].
14. J. Abraham *et al.* [Pierre Auger Collaboration], *Astropart. Phys.* **29**, 243-256 (2008).
15. J. Abraham *et al.* [Pierre Auger Collaboration], *Phys. Rev. Lett.* **100**, 211101 (2008).
16. J. Abraham *et al.* [Pierre Auger Collaboration], *Astropart. Phys.* **29**, 188 (2008); J. Abraham *et al.* [Pierre Auger Collaboration], *Science* **318**, 939 (2007).